The Solubility and Kinetics of Minerals under CO_2-EGS Geothermal Conditions: Comparison of Experimental and Modeling Results

Tianfu Xu[1], Patrick F. Dobson[1], and Miroslav Petro[2]

[1]Lawrence Berkeley National Laboratory (LBNL)
One Cyclotron Road, Berkeley, CA 94720

[2]Palo Alto Research Center (PARC)
3333 Coyote Hill Road, Palo Alto, CA 94304

Abstract

Although the thermal and hydraulic aspects of a CO_2-EGS system look promising, major uncertainties remain with regard to chemical interactions between fluids and rocks. A fully developed CO_2-based EGS would consist of three distinct zones: (1) a central zone or "core" (Zone 1) in which all aqueous phase has been removed by production or by dissolution into the flowing CO_2 stream, so that the reservoir fluid is a single supercritical CO_2 phase; (2) a surrounding intermediate zone (Zone 2), in which the reservoir fluid consists of a two-phase water-CO_2 mixture; and (3) an outer or peripheral zone (Zone 3), in which the reservoir fluid is a single aqueous phase with dissolved CO_2. Chemical reaction processes are expected to be quite different in the three zones.

Solubility and reaction kinetics of minerals are very important for understanding and predicting mineral alteration occurring in a CO_2-H_2O mixture (Zone 2) and under aqueous phase (Zone 3) conditions. Laboratory experiments were performed under both conditions for some major individual minerals that are likely encountered in a CO_2-EGS system. In order to gain insight into solubility and kinetics, here we present modeling analyses based on the evolution of observed aqueous species concentrations. The combined experimental and modeling study as presented in this paper could enable us to predict the coupled processes of fluid flow, heat transfer, and geochemical reactions, and then to evaluate the performance, risks and benefits of a CO_2-EGS operation.

Key words. CO_2-EGS, Mineral alteration, Mineral solubility, Reaction kinetics, Geochemical modeling, Supercritical CO_2.

1. Introduction

Enhanced Geothermal Systems (EGS) are defined as engineered reservoirs that have been created to extract economical amounts of heat from geothermal resources of low permeability and/or porosity (MIT, 2006). The MIT report indicated that EGS could become a major supplier of primary energy for U.S. base-load electrical generation capacity by 2050. In this study, we consider a novel EGS concept that would use carbon dioxide (CO_2) instead of water as the heat transmission fluid, and would achieve geologic sequestration of CO_2 as an ancillary benefit (Brown, 2000; Pruess, 2006).

Numerical simulations of fluid dynamics and heat transfer indicate that supercritical CO_2 is superior to water in its ability to mine heat from hot fractured rock (Pruess, 2006 and 2008). Carbon dioxide also offers advantages with respect to wellbore hydraulics, in that its lower viscosity and larger expansivity as compared to water would increase buoyancy forces and reduce the parasitic power consumption of the fluid circulation system. While the thermal and hydraulic aspects of a CO_2-EGS system look promising, major uncertainties remain with regard to chemical interactions between fluids and rocks, especially during its transition from water-dominated to dry CO_2-based system. As shown in Figure 1, a fully developed EGS with CO_2 would consist of three distinct zones (modified from Fouillac et al., 2004; Ueda et al., 2005), (1) a central zone or "core" (Zone 1) in which all aqueous phase has been removed by production and dissolution into the flowing CO_2 stream, so that the reservoir fluid is a single supercritical CO_2 phase; (2) a surrounding intermediate zone (Zone 2), in which the reservoir fluid consists of a two-phase water-CO_2 mixture; and (3) an outer or peripheral zone (Zone 3), in which the reservoir fluid is a single aqueous phase with dissolved CO_2.

Chemical processes are expected to be quite different in the three zones (Xu et al., 2008). The absence of water in the inner (core) zone poses unique questions, as little is presently known about the geochemistry of non-aqueous systems. The aqueous fluids initially present in an EGS reservoir would be removed by immiscible displacement by CO_2, and by dissolution (evaporation) into the flowing CO_2 stream. Continuous operation of a CO_2-EGS may produce a rather dry CO_2 stream. Research on reactions between supercritical CO_2 and rocks in the absence of water has started only recently (Regnault et al., 2005; McGrail et al., 2009). Carbon dioxide is not an ionic solvent, which would reduce the potential for dissolution and subsequent re-precipitation of minerals, and avoid problems of scaling and formation plugging (Brown, 2000). It appears likely that prolonged exposure to supercritical CO_2 could cause dehydration reactions that would remove loosely bound water from rock minerals (clay). Such reactions may reduce the molar volume of the minerals involved, which would increase the porosity and permeability of the formations, and might promote reservoir growth (Pruess and Azaroual, 2006).

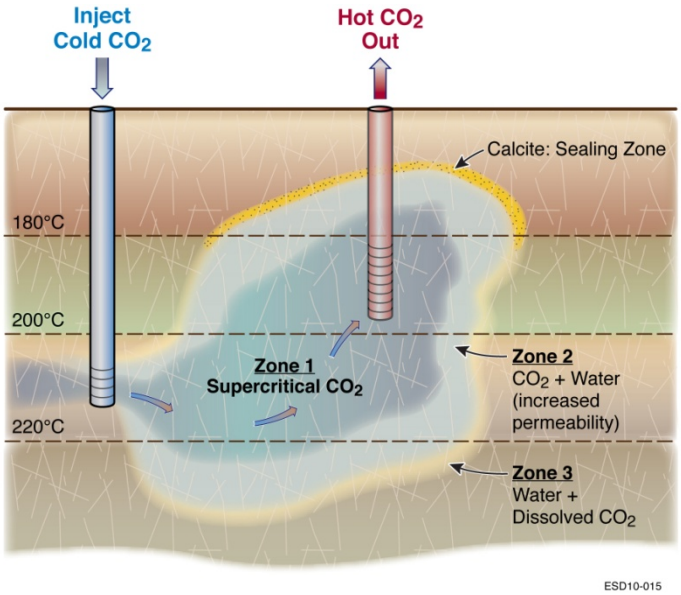

Figure 1. Schematic of the three zones created by injection of CO_2 into hot fractured rock (after Fouillac et al., 2004; Ueda et al., 2005).

Rock-fluid interactions in Zones 2 and 3 would be mediated by the aqueous phase. Some information on relevant processes is available from laboratory experiments (Ueda et al., 2005), natural CO_2-bearing geothermal systems (Giolito et al., 2007), and reactive chemical transport modeling (Gherardi et al., 2007). In Zone 2, the dominant process is mineral dissolution because of low pH induced by co-existing CO_2. The peripheral zone (Zone 3) of an EGS operated with CO_2 may experience a combination of mineral dissolution and precipitation effects that could impact reservoir growth and longevity. The long-term behavior of this outermost zone will be crucial for sustaining energy recovery, for estimating CO_2 loss rates, and for determining tradeoffs between power generation and geologic storage of CO_2.

Solubility and reaction kinetics of minerals are very important for understanding and predicting mineral alteration under CO_2-H_2O mixtures (Zone 2) and aqueous phase (Zone 3) conditions. For this reason, Palo Alto Research Center (PARC) has performed laboratory experiments under both conditions for some major individual minerals that are likely encountered in a CO_2-EGS system. In collaboration with PARC, Lawrence Berkeley National Laboratory (LBNL) has conducted modeling analyses for the measured data obtained by PARC using the LBNL in-house developed multiphase non-isothermal reactive transport simulator TOUGHREACT (Xu et al., 2011).

The new experimental results combined with modeling analyses, as presented in this paper, could enable us to evaluate and predict the flow of underground fluids and assess both risks and benefits of CO_2-EGS operations.

2. Experimental data review

Petro et al. (2012) has developed an integrated multichannel reactor system, which can be fed by a mixture of gases, liquids and supercritical fluids, and operate in a wide range of high-pressure and high-temperature conditions. When coupled to an on-line diagnostics system for real-time complex ion analysis under the reaction/interaction conditions, it produces data on individual ion concentrations over time, representing the dissolution profile of each mineral for a specific set of experimental conditions. The data can be combined into the overall mineral solubilities, or correlated with other parameters, including those important for modeling a specific geothermal site or condition. Table 1 shows a summary of selected data obtained for some minerals under study. While screening a broad combinatorial space of mineral solubilities, the experiments proceeded from conditions that have been reported by past studies to previously unexplored combinations of minerals, grain sizes, fluid environments, pressures, and temperatures.

Table 1. Individual ion concentrations for selected minerals as measured by PARC rock-fluid interaction system (updated from Petro et al., 2012).

Rock Sample				Fluid Environment		Reactor Conditions		Ion Analysis Results				
Sample Name	Mineral Composition	Particle Size Min (μm)	Particle Size Max (μm)	Water (vol.%)	CO2 (vol.%)	Temperature (oC)	Pressure (psi)	Ion Detected	Concentration at 20 hrs (mg/L)	Concentration at 40 hrs (mg/L)	Concentration at 60 hrs (mg/L)	Concentration at 80 hrs (mg/L)
Calcite	$Ca(CO)_3$	63	150	100	0	150	1200	Ca^{2+}		12	17	
	$Ca(CO)_3$	63	150	67	33	150	1200	Ca^{2+}			164	173
	$Ca(CO)_3$	63	150	56	44	150	1200	Ca^{2+}	155	175	186	194
	$Ca(CO)_3$	63	150	56	44	120	1200	Ca^{2+}	245	283	306	322
Dolomite	$MgCa(CO_3)_2$	63	150	100	0	150	1200	Mg^{2+}		3	4	
	$MgCa(CO_3)_2$	63	150	33	67	150	1200	Mg^{2+}	54			
	$MgCa(CO_3)_2$	63	150	67	33	150	1200	Mg^{2+}			50	53
	$MgCa(CO_3)_2$	63	150	56	44	120	1200	Mg^{2+}	76	86	92	
	$MgCa(CO_3)_2$	63	150	100	0	150	1200	Ca^{2+}		6	10	
	$MgCa(CO_3)_2$	63	150	33	67	150	1200	Ca^{2+}	111			
	$MgCa(CO_3)_2$	63	150	67	33	150	1200	Ca^{2+}			93	99
	$MgCa(CO_3)_2$	63	150	56	44	120	1200	Ca^{2+}	151	171	182	
Labradorite	$(Ca,Na)(Si,Al)_4O_8$	63	150	100	0	150	1200	Ca^{2+}		4	5	
	$(Ca,Na)(Si,Al)_4O_8$	63	150	33	67	150	1200	Ca^{2+}	34			
	$(Ca,Na)(Si,Al)_4O_8$	63	150	67	33	150	1200	Ca^{2+}			38	41
	$(Ca,Na)(Si,Al)_4O_8$	63	150	56	44	120	1200	Ca^{2+}	21	24	26	
	$(Ca,Na)(Si,Al)_4O_8$	63	150	100	0	150	1200	Na^{+}	1	1	2	3
	$(Ca,Na)(Si,Al)_4O_8$	63	150	67	33	150	1200	Na^{+}				11
	$(Ca,Na)(Si,Al)_4O_8$	63	150	56	44	150	1200	Na^{+}			6	
	$(Ca,Na)(Si,Al)_4O_8$	63	150	33	67	150	1200	Na^{+}	7			
Microcline	$KAlSi_3O_8$	25	63	100	0	120	1200	K^{+}	8	9	10	10
	$KAlSi_3O_8$	25	63	100	0	150	1200	K^{+}	5	6	6	7
	$KAlSi_3O_8$	25	63	56	44	150	1200	K^{+}	9	10	11	12
	$KAlSi_3O_8$	25	63	56	44	120	1200	K^{+}	7	8	9	10
Siderite	$FeCO_3$	25	63	100	0	120	1200	Fe^{2+}	12	13	15	15
	$FeCO_3$	25	63	100	0	150	1200	Fe^{2+}	10	11	12	12
	$FeCO_3$	25	63	56	44	150	1200	Fe^{2+}	44	52	56	59
	$FeCO_3$	25	63	56	44	120	1200	Fe^{2+}	48	54	58	61
Biotite	$K(Mg,Fe)_3AlSi_3O_{10}(F,OH)_2$	25	63	100	0	120	1200	K^{+}	7	8	9	9
	$K(Mg,Fe)_3AlSi_3O_{10}(F,OH)_2$	25	63	100	0	150	1200	K^{+}	9	10	10	11
	$K(Mg,Fe)_3AlSi_3O_{10}(F,OH)_2$	25	63	56	44	150	1200	K^{+}	23	26	28	30
	$K(Mg,Fe)_3AlSi_3O_{10}(F,OH)_2$	25	63	56	44	120	1200	K^{+}	24	28	30	31
	$K(Mg,Fe)_3AlSi_3O_{10}(F,OH)_2$	25	63	100	0	120	1200	Fe^{2+}	14	16	18	19
	$K(Mg,Fe)_3AlSi_3O_{10}(F,OH)_2$	25	63	100	0	150	1200	Fe^{2+}	14	16	17	18
	$K(Mg,Fe)_3AlSi_3O_{10}(F,OH)_2$	25	63	56	44	150	1200	Fe^{2+}	59	67	72	76
	$K(Mg,Fe)_3AlSi_3O_{10}(F,OH)_2$	25	63	56	44	120	1200	Fe^{2+}	66	75	80	84
	$K(Mg,Fe)_3AlSi_3O_{10}(F,OH)_2$	25	63	100	0	120	1200	Mg^{2+}	22	26	28	30
	$K(Mg,Fe)_3AlSi_3O_{10}(F,OH)_2$	25	63	100	0	150	1200	Mg^{2+}	18	20	22	23
	$K(Mg,Fe)_3AlSi_3O_{10}(F,OH)_2$	25	63	56	44	150	1200	Mg^{2+}	34	38	41	43
	$K(Mg,Fe)_3AlSi_3O_{10}(F,OH)_2$	25	63	56	44	120	1200	Mg^{2+}	34	39	42	44

3. Modeling results and discussion

Using the same experimental conditions of pressure and temperature, we performed TOUGHREACT numerical modeling analyses for some specific minerals selected, and compared the simulation results with measured data.

A general form of rate expression was used in the TOUGHREACT program (see Appendix A), which is based on transition state theory (TST) (Lasaga et al., 1994; Steefel and Lasaga, 1994). Mineral dissolution and/or precipitation rates are a product of the kinetic-rate constant and reactive surface area as represented by Eq. A.1. The parameters used for calculating the kinetic-rate constant are given in Table 2. In Table 2, we include separate rate constants (k_{25}), activation energies (E), and reaction order (n) for processes catalyzed by H^+ or OH^-. At any pH, the total rate is the sum of the rates from all mechanisms. Catalysis by H^+ or OH^- is considered only for mineral dissolution. Rate-constant related parameters for the rate law were taken from Palandri and Kharaka (2004), who compiled and fitted experimental data reported by many investigators, as well as Steefel (2001). Most solubility products for minerals were taken from the EQ3/6 V7.2b database (Wolery, 1992).

Modeling results together with measured data for selected individual minerals are presented as follows.

3.1. Calcite

For the condition of water only (similar to Zone 3 of a CO_2-EGS system) at 150°C, modeled Ca concentrations (generated from calcite dissolution) over time together with measured values are presented in Figure 2a. The initial modeled curve (red line) is below measured data. Calcite solubility is highly dependent on CO_2 partial pressure (Pco_2). In the case of a laboratory experiment using pure water, incomplete removal of dissolved CO_2 from the atmosphere may result in the presence of small amounts of CO_2. Therefore, we attempted to specify a Pco_2 value, in order to reproduce the observed profile. Using a Pco_2 of 0.12 bar in the simulation gives a good match between the two data sets.

In the current modeling calibration, we only changed reactive surface area but kept other rate-constant related parameters unchanged. The initial guess and calibrated values of the specific reactive surface areas (A) are given in Table 3. The match of Ca concentrations at 150 ^{o}C was achieved by reducing the initial-guess A from 9.8 cm^2/g to 6.2×10^{-5} cm^2/g. Note that the dissolution rate is equal to rate constant (k) multiplied by surface area (A). The reduced areas could be due to the fact that the rate-constant (k) is much smaller in the experiment than the value given in Table 2.

The geometric reactive surface areas A_g of mineral grains used in the experiments (m^2/m^3 mineral = 1/m) are calculated from: $A_g = 6/d$ (Perez and Boles, 2005; assuming grain density of albite) with correction of the density of each minerals, where d is the grain diameter (m). In the experiments, the particle sizes range from 25 to 150 µm (See Table 1). Based on these grain sizes (and considering grain densities for each mineral used), the geometric surface areas range from 101 to 927 cm^2/g, which is much larger than the calibrated reactive surface areas.

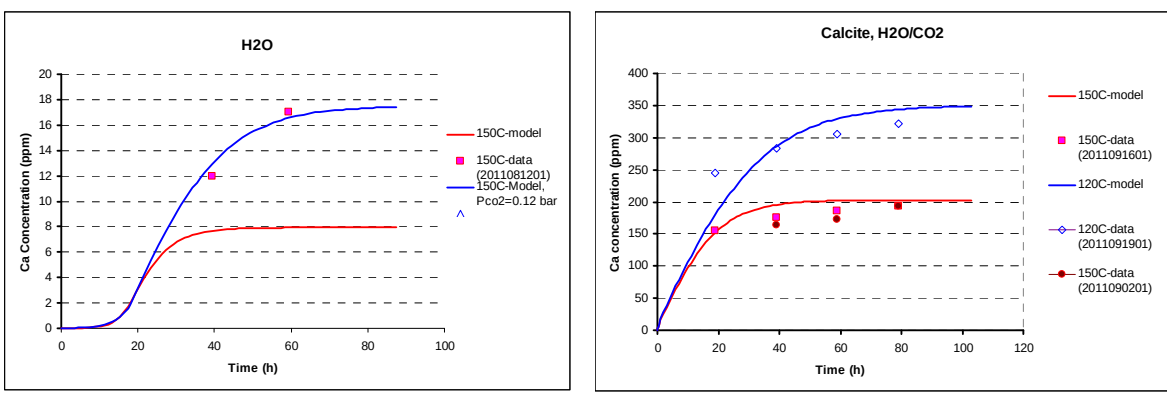

(a) Water only (b) Water/CO_2 mixture

Figure 2. Modeled Ca concentrations over time obtained from calcite dissolution at 120 and 150°C together with measured values from the experiments.

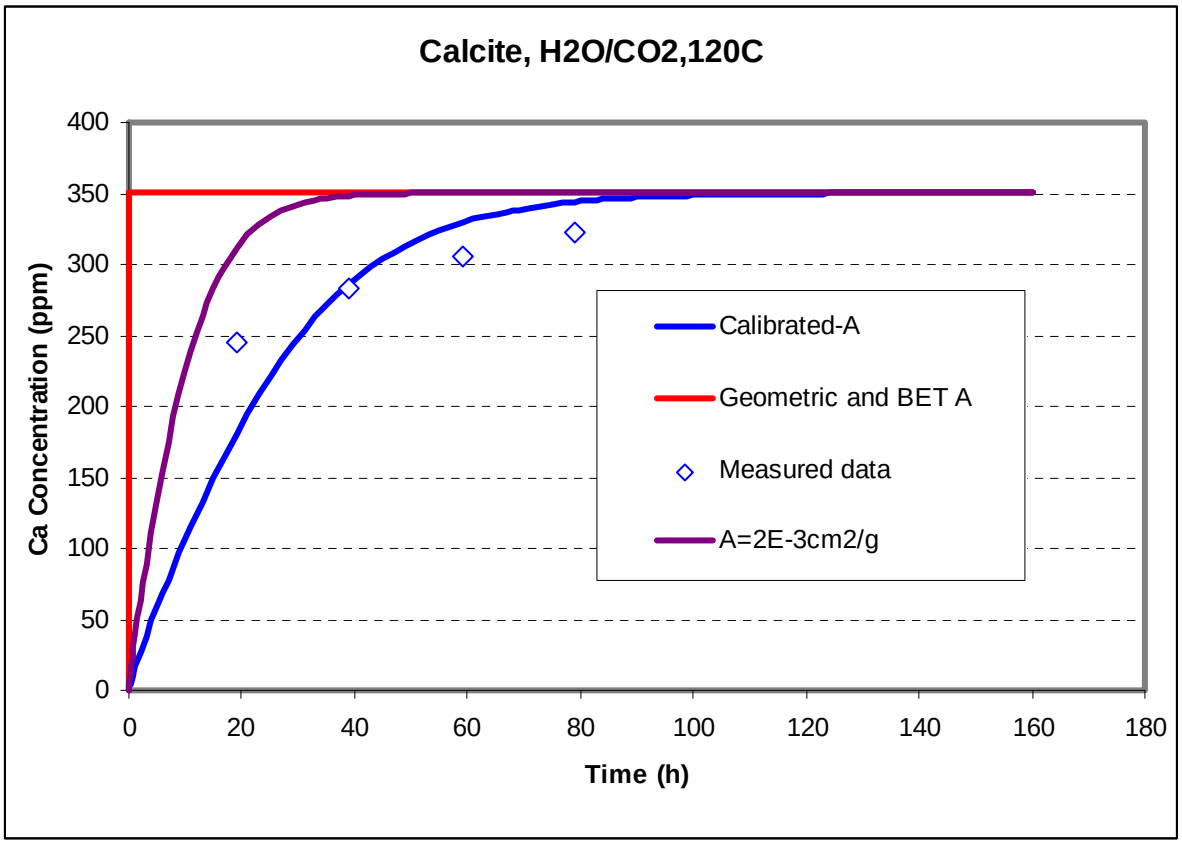

Table 2. Parameters for calculating kinetic rate constants of selected minerals. Note that: (1) all rate constants are listed for dissolution; (2) k_{25} is kinetic constant at 25°C, E_a is activation energy, and n is the power term (Eq. A.2); (3) the power term n for both acid and base mechanisms are with respect to H^+.

Mineral	Parameters for kinetic rate law							
	Neutral mechanism		Acid mechanism			Base mechanism		
	k_{25} (mol/m^2/s)	E_a (KJ /mol)	k_{25}	E_a	n(H^+)	k_{25}	E_a	n(H^+)
***Primary*:**								
Calcite[1]	1.549×10^{-6}	23.5	5.012×10^{-1}	14.4	1.0			
Siderite[2]	1.260×10^{-9}	62.76	1.590×10^{-4}	45.0	0.9			
Labradorite[1]	1.230×10^{-11}	45.2	1.349×10^{-8}	42.1	0.626			
Dolomite[1]	2.951×10^{-8}	52.2	6.457×10^{-4}	36.1	0.5			
Microcline[1]	3.890×10^{-13}	38	8.710×10^{-11}	51.7	0.5	6.310×10^{-22}	94.1	-0.823
Biotite[1]	2.818×10^{-13}	22.0	1.445×10^{-10}	22.0	0.525			

1- Palandri and Kharaka, 2004; 2 – Steefel, 2001

Table 3. Initial guess and calibrated surface areas of minerals.

Mineral	Cases	Grain size range (cm)	A (cm^2/g) **Geometric** (average)	A (cm^2/g) **BET**	A (cm^2/g) **Calibrated**
***Primary*:**					
Calcite	H_2O, 150°C	0.0063-0.015	250	15(5887)	6.2×10^{-5}
	H_2O, 150°C, Pco2=0.12 bar				6.2×10^{-5}
	H_2O-CO_2, 120°C				7.8×10^{-4}
	H_2O-CO_2, 150°C				4.8×10^{-4}
Siderite	H_2O, 150°C	0.0025-0.0063	423		6.2×10^{-5}
	H_2O-CO_2, 120°C				5.5×10^{-6}
	H_2O-CO_2, 150°C				5.5×10^{-6}
Labradorite	H_2O, 150°C	0.0063-0.015	250		1.3×10^{-2}
	H_2O-CO_2, 120°C				8.0×10^{-1}
	H_2O-CO_2, 150°C				3.0×10^{-1}
Dolomite					
	H_2O-CO_2, 120°C	0.0063-0.015	236	428	4.5×10^{-5}
	H_2O-CO_2, 150°C				4.5×10^{-5}
Microcline	H_2O, 120°C	0.0025-0.0063	647	3120	60
	H_2O, 150°C				60
	H_2O-CO_2, 120°C				60
	H_2O-CO_2, 150°C				60
Biotite					
	H_2O-CO_2, 120°C	0.0025-0.0063	559	2689	125
	H_2O-CO_2, 150°C				125

For cases with mixing H_2O/CO_2 and a pressure of 1200 psi, modeled Ca concentrations over time obtained with 120 and 150°C temperatures together with measured data for four experiments are presented in Figure 2b. For 120°C, the modeled curve is close to experimental data performed on 09/19/2011 (ID: 2011091901). The modeled results for 150°C reproduce reasonably well the experimental data on 09/16/2011. Note that for models at two different temperatures, the calibrated reactive surface areas are different (see Table 3). This may imply that the kinetic rate constant at 150°C is smaller than that at 120°C for calcite.

3.2. Siderite

Under water-only conditions, modeled Fe concentrations due to dissolution of siderite are much lower that those of measured values (Figure 3a). These could result from (1) CO_2 partial pressure effect as discussed in the previous calcite case, and (2) corrosion of iron-bearing equipment used in the experiment. Under water/CO_2 mixture conditions (Figure 3b), siderite solubility in terms of Fe concentration is about five times larger than those under water-only conditions. For the temperature of 120°C, the modeled Fe concentration curve reproduces reasonably well the measured data. For the temperature of 150°C, the modeled Fe curve is lower than the measured data.

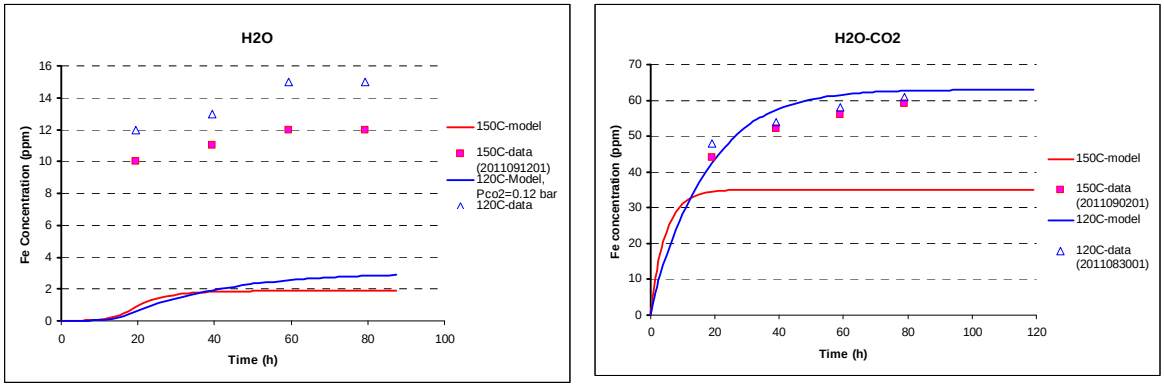

(a) Water only

(b) Water/CO_2 mixture

Figure 3. Modeled Fe concentrations over time obtained from siderite dissolution at 120 and 150°C together with measured data from the experiments.

3.3. Labradorite

Under water-only conditions at a temperature of 150°C, modeled Ca concentrations due to dissolution of labradorite reproduces very well the measured points (Figure 4a). The modeled Na curve captures the measured data at 20 and 80 hours, but is off from the data at 40 and 60 hours (Figure 4b). Under water/CO_2 mixture conditions, at a temperature of 120°C the modeled Ca concentrations are close to the experimental data, but at a temperature of 150°C modeled Ca concentrations are much lower than the data (Figure 4c). The modeled Na curve at 120°C captures the data at the final time of 80 hours (Figure 4d).

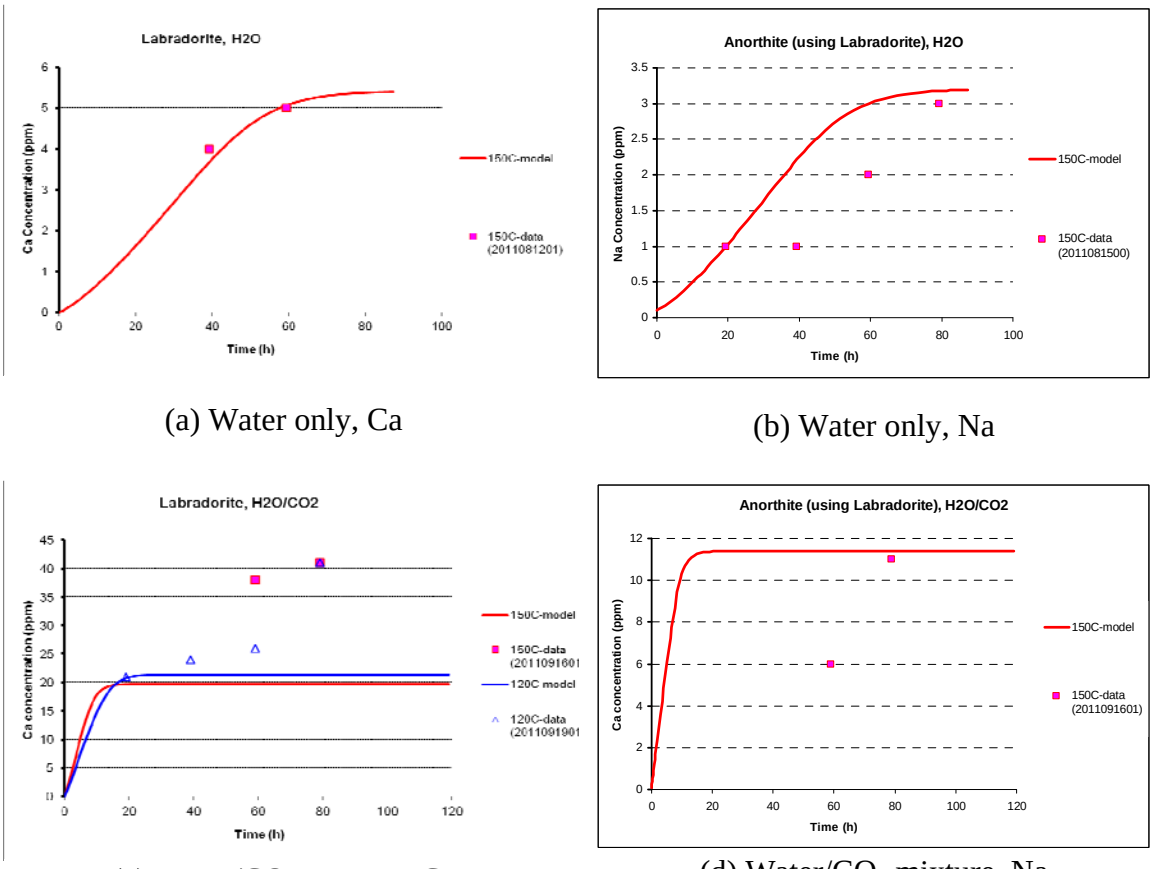

(a) Water only, Ca

(b) Water only, Na

(c) Water/CO_2 mixture, Ca

(d) Water/CO_2 mixture, Na

Figure 4. Modeled Ca and Na concentrations over time obtained from labradorite dissolution at 120 and 150°C together with measured values from the experiments.

3.4. Microcline

Under water-only conditions, modeled K concentrations due to dissolution of microcline reproduce quite well the measured data for both 120 and 150°C (Figure 5a). Under water/CO_2 mixture conditions, for 120°C the modeled curve of K concentration can capture somewhat measured data, but for 150°C the simulations predict K concentrations that are much higher than the measured data (Figure 5b).

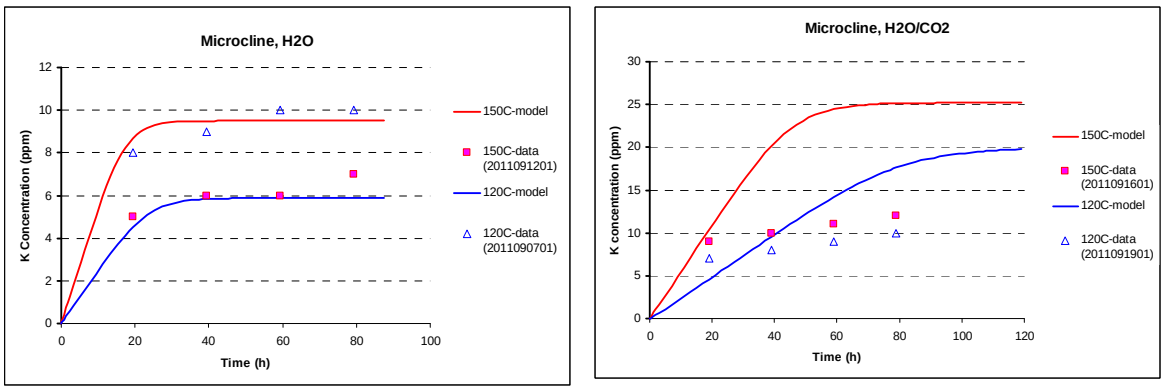

(a) Water only

(b) Water/CO_2 mixture

Figure 5. Modeled K concentrations over time obtained from microcline dissolution at 120 and 150°C under both water-only (a) and water/CO_2 mixture (b) conditions together with experimental data.

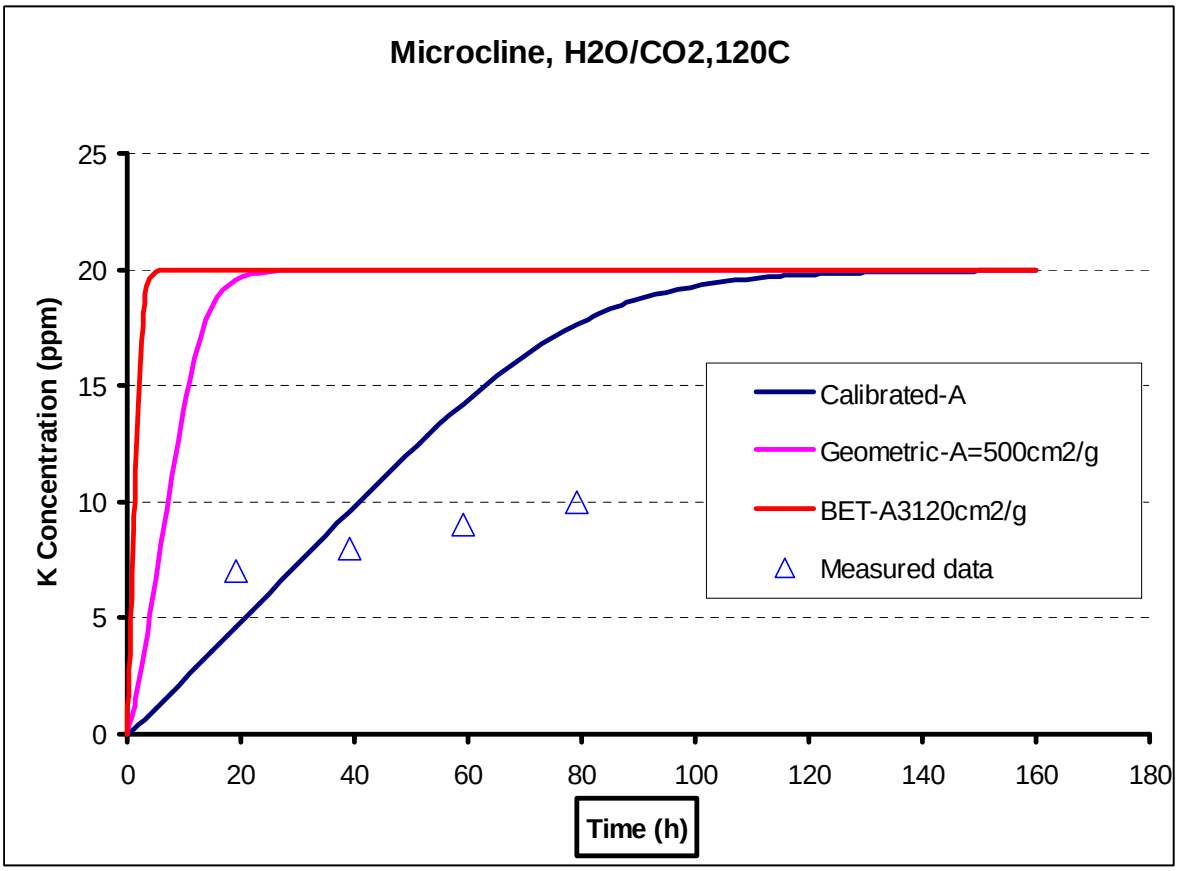

3.5. Dolomite

Under water-only conditions, modeled dissolved concentrations from dolomite dissolution are close to the measured points. Under water/CO_2 mixture conditions, modeled Mg and Ca concentrations from dolomite dissolution compares quite well with the measured data (Figures 6a and 6b).

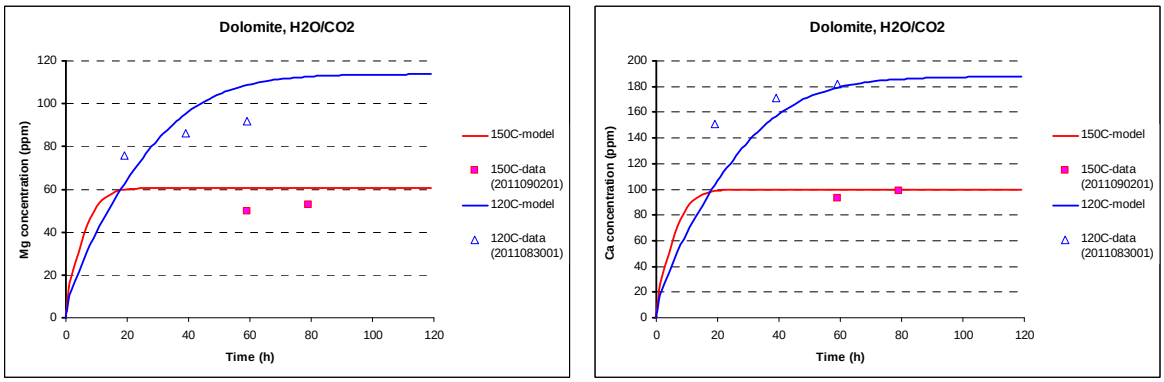

(a) Mg (b) Ca

Figure 6. Modeled concentrations of Mg (a) and Ca (b) over time obtained from dolomite dissolution at 120 and 150°C under water/CO_2 mixture condition together with experimental data.

3.6. Biotite

Under water/CO_2 mixture conditions, modeled dissolved Fe concentrations from biotite dissolution at 150°C compares very well with measured data, but at 120°C the modeled curve is much higher than the measured points (Figure 7a). Modeled Mg concentrations at 150°C are lower than measured data, but at 120°C the modeled curve is higher (Figure 7b), biotite solubilities in terms of dissolved Mg at both temperatures are similar.

Modeled K concentrations at 150°C are slightly higher than the measured data, but at 120°C the modeled curve is much higher (Figure 7c), biotite solubilities in terms of dissolved K at both temperatures are also similar. In water-only conditions, most silicates have increasing solubilities with increasing temperature. However, here with the presence of CO_2, the modeled concentrations of K, Mg, and Fe are higher for the 120°C runs than the 150 ^{o}C runs. This is likely because at higher temperatures CO_2 solubility is lower and then pH is higher and both temperature and pH significantly affect mineral solubilities.

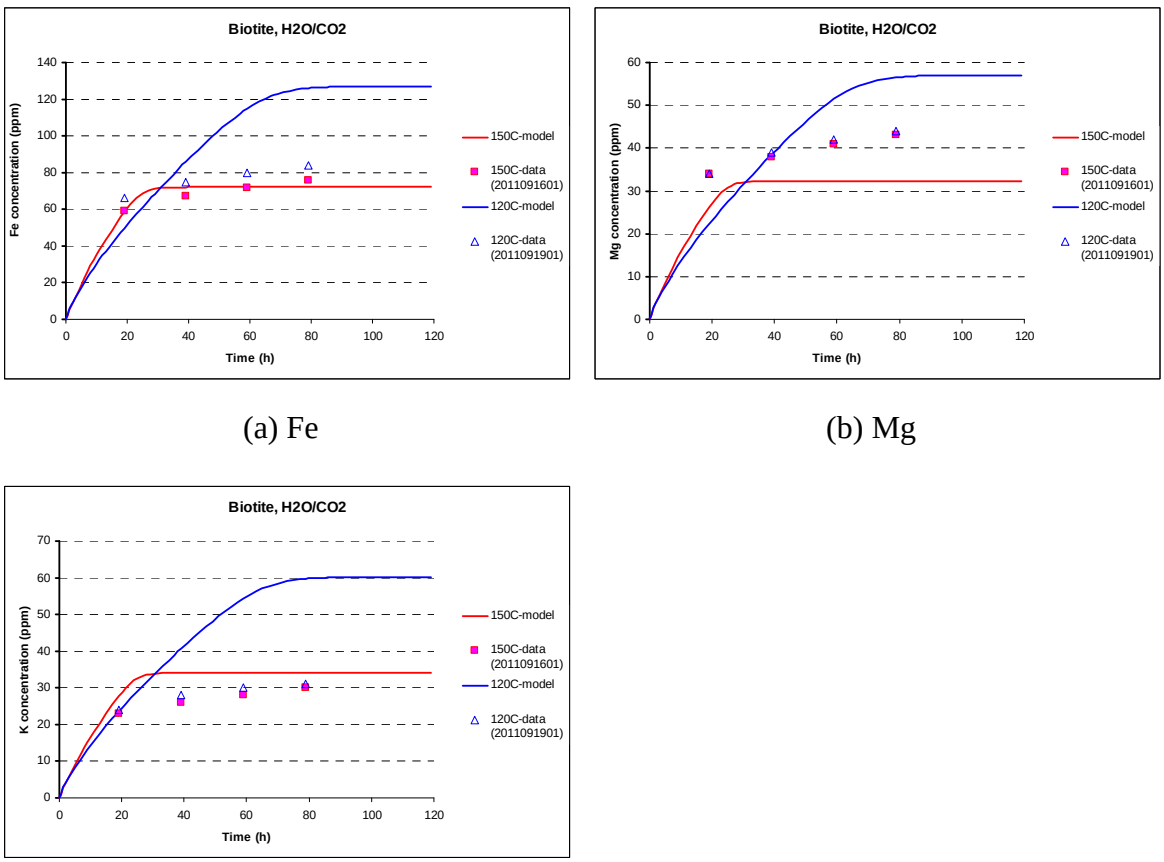

(a) Fe (b) Mg

(c) K

Figure 7. Modeled concentrations of Fe (a), Mg (b) and K (c) over time obtained from biotite dissolution at 120 and 150°C under water/CO_2 mixture conditions together with the corresponding experimental data.

4. Conclusions

Based on the evolution of aqueous concentrations of selected cations in solutions derived from mineral dissolution experiments, we have performed TOUGHREACT batch geochemical modeling analyses and calibration. Most measured ion concentrations can be captured by the modeling with calibration of reaction kinetic parameters, indicating solubility data in the database are mostly accurate. Under water-only conditions (similar to Zone 3 of a CO_2-EGS system), carbonate minerals such as calcite, siderite and dolomite are less soluble in the model. This could be due to minor amounts of CO_2 present in the water which was not characterized in the experiment. Some differences of modeling solubility from measured data may be due to: (1) errors in the measured values, (2) effects from the equipment such as iron corrosion, (3) problems with the solubility and kinetic values for minerals used in the simulations, (4) impurities in the minerals, and (5) possible formation of complexes that may affect the solubilities of remaining mineral components, like with aluminosilicates at elevated P_{CO2}. The exact reason for the differences should be determined in ongoing/future modeling and experimental studies. Future modeling efforts will work to incorporate these complexes into the system. Under water/CO_2 mixture (Zone 2) conditions, solubilities for all minerals are higher than those under water-only condition (Zone 3). Therefore, in Zone 2 of a CO_2-EGS system, the effects of mineral dissolution and precipitation are very strong, likely resulting in changes in reservoir physical properties such as porosity and permeability. The combined experimental and modeling study as presented in this paper could enable us to predict the coupled processes of fluid flow, heat transfer, and geochemical reactions, and then to evaluate the performance, risks, and benefits of a CO_2-EGS operation.

Acknowledgments. We thank Frank Monastero for his careful review of the manuscript. This work was supported by Lawrence Berkeley National Laboratory under Department of Energy Contract No. DE-AC02-05CH11231, and in collaboration with Palo Alto Research Center (PARC) through the U.S. Department of Energy, Geothermal Technologies Program, Energy Efficiency and Renewable Energy Office, Award No. DE-EE0002765.

References

Brown, D., 2000. A Hot Dry Rock geothermal energy concept utilizing supercritical CO_2 instead of water. Proceedings, 25th Workshop on Geothermal Reservoir Engineering, Stanford University, pp. 233–238.

Fouillac, C., Sanjuan, B., Gentier, S., and Czernichowski-Lauriol, I., 2004. Could sequestration of CO_2 be combined with the development of Enhanced Geothermal Systems? Third Annual Conference on Carbon Capture and Sequestration, Alexandria, VA.

Gherardi, F., Xu, T., and Pruess, K., 2007. Numerical modeling of self-limiting and self-enhancing caprock alteration induced by CO_2 storage in a depleted gas reservoir. Chem. Geol. 244, 103–129.

Giolito, Ch., Ruggieri, G., and Gianelli, G., 2007. Fluid evolution in the deep reservoir of the Mt. Amiata Geothermal Field, Italy, Transactions, Geothermal Resources Council, 31, 153-158.

Lasaga, A.C., Soler, J.M., Ganor, J., Burch, T.E., and Nagy, K.L., 1994. Chemical weathering rate laws and global geochemical cycles. Geochimica et Cosmochimica Acta 58, 2361-2386.

McGrail, B.P., Schaef, H.T., Glezakou, V.-A., Dang, L.X., and Owen, A.T., 2009. Water Reactivity in the Liquid and Supercritical CO_2 Phase: Has Half the Story Been Neglected? Energy Procedia 1, 3415–3419.

MIT, 2006. The Future of Geothermal Energy Impact of Enhanced Geothermal Systems (EGS) on the United States in the 21st Century. A Report for the U.S. Department of Energy, Massachusetts Institute of Technology.

Palandri, J., Kharaka, Y.K., 2004. A compilation of rate parameters of water-mineral interaction kinetics for application to geochemical modeling. US Geol. Surv. Open File Report 2004-1068, 64 pp.

Perez, R.J. Boles J.R., 2005. An empirically derived kinetic model for albitization of detrital plagioclase, American Journal of Science 305, 312–343.

Petro, M., Song, L., Bell, A., Tuganov, A., Parajuly, K., Dobson, P., Xu, T., and Pruess, K., 2012. System and methodology for rapid evaluation of geothermal rock-fluid interactions Proceedings, 37th Workshop on Geothermal Reservoir Engineering, Stanford University, Stanford, California, January 30-February 1, 2012.

Pruess, K., 2006. Enhanced Geothermal Systems (EGS) Using CO_2 as Working Fluid - A Novel Approach for Generating Renewable Energy With Simultaneous Sequestration of Carbon. Geothermics 35, 351–367.

Pruess, K., and Azaroual, M., 2006. On the feasibility of using supercritical CO_2 as heat transmission fluid in an engineered hot dry rock geothermal system. Proceedings, 31st Workshop on Geothermal Reservoir Engineering, Stanford University, Stanford, CA, USA, pp. 386–393.

Pruess, K., 2008. On production behavior of enhanced geothermal systems with CO_2 as Working Fluid. Energy Conversion and Management 49, 1446–1454.

Regnault, O., Lagneau, V., Catalette, H., and Schneider, H., 2005. Étude Expérimentale de la Réactivité du CO_2 Supercritique vis-à-vis de Phases Minérales pures. Implications pour la Sequestration Géologique de CO_2. C. R. Geoscience 337, 1331–1339.

Steefel, C.I., and Lasaga, A.C., 1994. A coupled model for transport of multiple chemical species and kinetic precipitation/dissolution reactions with applications to reactive flow in single phase hydrothermal system. American Journal of Science 294, 529–592.

Steefel, C.I., 2001. CRUNCH. Lawrence Livermore National Laboratory, p. 76.

Ueda, A., Kato, K., Ohsumi, T., Yajima, T., Ito, H., Kaieda, H., Meycalf, R., and Takase, H., 2005. Experimental studies of CO_2-rock interaction at elevated temperatures under hydrothermal conditions. Geochem. J. 39, 417–425.

Wolery, T. J., 1992. EQ3/6: Software package for geochemical modeling of aqueous systems: Package overview and installation guide (version 7.0), Lawrence Livermore National Laboratory Report UCRL-MA-110662 PT I, Livermore, California,.

Xu, T., Pruess, K., and Apps, J., 2008. Numerical studies of fluid-rock interactions in enhanced geothermal systems (EGS) with CO_2 as working fluid. Proceedings, 33rd Workshop on Geothermal Reservoir Engineering Stanford University, Stanford, California, January 28-30.

Xu, T., Spycher, N., Sonnenthal, E.L., Zhang, G., Zheng, L., Pruess, K., 2011. TOUGHREACT Version 2.0: A simulator for subsurface reactive transport under non-isothermal multiphase flow conditions. Computers & Geosciences 37, 763–774.

Appendix A. Kinetic rate law for mineral dissolution and precipitation

The general rate expression used in TOUGHREACT is taken from Lasaga et al. (1994) and Steefel and Lasaga (1994):

$$r_n = \pm k_n A_n \left| 1 - \left(\frac{Q_n}{K_n} \right)^{\theta} \right|^{\eta} \tag{A.1}$$

where n denotes kinetic mineral index, positive values of r_n indicate dissolution and negative values precipitation, k_n is the rate constant (moles per unit mineral surface area and unit time) which is temperature dependent, A_n is the specific reactive surface area, K_n is the equilibrium constant for the mineral-water reaction written for the destruction of one mole of mineral n, and Q_n is the reaction quotient. The parameters θ and η must be determined from experiments; usually, but not always, they are taken equal to one.

For many minerals, the kinetic rate constant k can be summed from three different mechanisms (Lasaga et al., 1994; Palandri and Kharaka, 2004):

$$\begin{aligned} k = k_{25}^{nu} \exp\left[\frac{-E_a^{nu}}{R} \left(\frac{1}{T} - \frac{1}{298.15} \right) \right] + k_{25}^{H} \exp\left[\frac{-E_a^{H}}{R} \left(\frac{1}{T} - \frac{1}{298.15} \right) \right] a_H^{n_H} \\ + k_{25}^{OH} \exp\left[\frac{-E_a^{OH}}{R} \left(\frac{1}{T} - \frac{1}{298.15} \right) \right] a_{OH}^{n_{OH}} \end{aligned} \tag{A.2}$$

where superscripts or subscripts nu, H, and OH indicate neutral, acid and base mechanisms, respectively, E_a is the activation energy, k_{25} is the rate constant at 25°C, R is gas constant (8.314 J mol^{-1} K^{-1}), T is absolute temperature (K), a is the activity of the species; and n is power term (constant). Notice that parameters θ and η (see Eq. A.1) are assumed the same for each mechanism.

DISCLAIMER

This document was prepared as an account of work sponsored by the United States Government. While this document is believed to contain correct information, neither the United States Government nor any agency thereof, nor The Regents of the University of California, nor any of their employees, makes any warranty, express or implied, or assumes any legal responsibility for the accuracy, completeness, or usefulness of any information, apparatus, product, or process disclosed, or represents that its use would not infringe privately owned rights. Reference herein to any specific commercial product, process, or service by its trade name, trademark, manufacturer, or otherwise, does not necessarily constitute or imply its endorsement, recommendation, or favoring by the United States Government or any agency thereof, or The Regents of the University of California. The views and opinions of authors expressed herein do not necessarily state or reflect those of the United States Government or any agency thereof or The Regents of the University of California.

Ernest Orlando Lawrence Berkeley National Laboratory is an equal opportunity employer.